

Pion Interferometry in Au+Au and Cu+Cu Collisions at RHIC

B. I. Abelev,⁸ M. M. Aggarwal,³⁰ Z. Ahammed,⁴⁷ B. D. Anderson,¹⁸ D. Arkhipkin,¹² G. S. Averichev,¹¹ J. Balewski,²² O. Barannikova,⁸ L. S. Barnby,² J. Baudot,¹⁶ S. Baumgart,⁵² D. R. Beavis,³ R. Bellwied,⁵⁰ F. Benedosso,²⁷ M. J. Betancourt,²² R. R. Betts,⁸ A. Bhasin,¹⁷ A. K. Bhati,³⁰ H. Bichsel,⁴⁹ J. Bielcik,¹⁰ J. Bielcikova,¹⁰ B. Biritz,⁶ L. C. Bland,³ M. Bombara,² B. E. Bonner,³⁶ M. Botje,²⁷ J. Bouchet,¹⁸ E. Braidot,²⁷ A. V. Brandin,²⁵ E. Bruna,⁵² S. Bueltmann,²⁹ T. P. Burton,² M. Bystersky,¹⁰ X. Z. Cai,⁴⁰ H. Caines,⁵² M. Calderón de la Barca Sánchez,⁵ O. Catu,⁵² D. Cebra,⁵ R. Cendejas,⁶ M. C. Cervantes,⁴² Z. Chajecski,²⁸ P. Chaloupka,¹⁰ S. Chattopadhyay,⁴⁷ H. F. Chen,³⁸ J. H. Chen,¹⁸ J. Y. Chen,⁵¹ J. Cheng,⁴⁴ M. Cherney,⁹ A. Chikanian,⁵² K. E. Choi,³⁴ W. Christie,³ R. F. Clarke,⁴² M. J. M. Codrington,⁴² R. Corliss,²² T. M. Cormier,⁵⁰ M. R. Cosentino,³⁷ J. G. Cramer,⁴⁹ H. J. Crawford,⁴ D. Das,⁵ S. Dash,¹³ M. Daugherty,⁴³ L. C. De Silva,⁵⁰ T. G. Dedovich,¹¹ M. DePhillips,³ A. A. Derevschikov,³² R. Derradi de Souza,⁷ L. Didenko,³ P. Djawotho,⁴² S. M. Dogra,¹⁷ X. Dong,²¹ J. L. Drachenberg,⁴² J. E. Draper,⁵ F. Du,⁵² J. C. Dunlop,³ M. R. Dutta Mazumdar,⁴⁷ W. R. Edwards,²¹ L. G. Efimov,¹¹ E. Elhalhuli,² M. Elnimr,⁵⁰ V. Emelianov,²⁵ J. Engelage,⁴ G. Eppley,³⁶ B. Erazmus,⁴¹ M. Estienne,¹⁶ L. Eun,³¹ P. Fachini,³ R. Fatemi,¹⁹ J. Fedorisin,¹¹ A. Feng,⁵¹ P. Filip,¹² E. Finch,⁵² V. Fine,³ Y. Fisyak,³ C. A. Gagliardi,⁴² L. Gaillard,² D. R. Gangadharan,⁶ M. S. Ganti,⁴⁷ E. J. Garcia-Solis,⁸ Geromitsos,⁴¹ F. Geurts,³⁶ V. Ghazikhanian,⁶ P. Ghosh,⁴⁷ Y. N. Gorbunov,⁹ A. Gordon,³ O. Grebenyuk,²¹ D. Grosnick,⁴⁶ B. Grube,³⁴ S. M. Guertin,⁶ K. S. F. F. Guimaraes,³⁷ A. Gupta,¹⁷ N. Gupta,¹⁷ W. Guryn,³ B. Haag,⁵ T. J. Hallman,³ A. Hamed,⁴² J. W. Harris,⁵² W. He,¹⁵ M. Heinz,⁵² S. Heppelmann,³¹ B. Hippolyte,¹⁶ A. Hirsch,³³ E. Hjort,²¹ A. M. Hoffman,²² G. W. Hoffmann,⁴³ D. J. Hofman,⁸ R. S. Hollis,⁸ H. Z. Huang,⁶ T. J. Humanic,²⁸ G. Igo,⁶ A. Iordanova,⁸ P. Jacobs,²¹ W. W. Jacobs,¹⁵ P. Jakl,¹⁰ C. Jena,¹³ F. Jin,⁴⁰ C. L. Jones,²² P. G. Jones,² J. Joseph,¹⁸ E. G. Judd,⁴ S. Kabana,⁴¹ K. Kajimoto,⁴³ K. Kang,⁴⁴ J. Kapitan,¹⁰ D. Keane,¹⁸ A. Kechechyan,¹¹ D. Kettler,⁴⁹ V. Yu. Khodyrev,³² D. P. Kikola,²¹ J. Kiryluk,²¹ A. Kisiel,²⁸ S. R. Klein,²¹ A. G. Knospe,⁵² A. Kocoloski,²² D. D. Koetke,⁴⁶ M. Kopytine,¹⁸ W. Korsch,¹⁹ L. Kotchenda,²⁵ V. Kouchpil,¹⁰ P. Kravtsov,²⁵ V. I. Kravtsov,³² K. Krueger,¹ M. Krus,¹⁰ C. Kuhn,¹⁶ L. Kumar,³⁰ P. Kurnadi,⁶ M. A. C. Lamont,³ J. M. Landgraf,³ S. LaPointe,⁵⁰ J. Lauret,³ A. Lebedev,³ R. Lednicky,¹² C-H. Lee,³⁴ J. H. Lee,³ W. Leight,²² M. J. LeVine,³ Li,⁵¹ C. Li,³⁸ Y. Li,⁴⁴ G. Lin,⁵² S. J. Lindenbaum,²⁶ M. A. Lisa,²⁸ F. Liu,⁵¹ J. Liu,³⁶ L. Liu,⁵¹ T. Ljubicic,³ W. J. Llope,³⁶ R. S. Longacre,³ W. A. Love,³ Y. Lu,³⁸ T. Ludlam,³ G. L. Ma,⁴⁰ Y. G. Ma,⁴⁰ D. P. Mahapatra,¹³ R. Majka,⁵² O. I. Mall,⁵ L. K. Mangotra,¹⁷ R. Manweiler,⁴⁶ S. Margetis,¹⁸ C. Markert,⁴³ H. S. Matis,²¹ Yu. A. Matulenko,³² T. S. McShane,⁹ A. Meschanin,³² R. Milner,²² N. G. Minaev,³² S. Mioduszewski,⁴² A. Mischke,²⁷ J. Mitchell,³⁶ B. Mohanty,⁴⁷ D. A. Morozov,³² M. G. Munhoz,³⁷ B. K. Nandi,¹⁴ C. Nattrass,⁵² T. K. Nayak,⁴⁷ J. M. Nelson,² P. K. Netrakanti,³³ M. J. Ng,⁴ L. V. Nogach,³² S. B. Nurushev,³² G. Odyniec,²¹ A. Ogawa,³ H. Okada,³ V. Okorokov,²⁵ D. Olson,²¹ M. Pachr,¹⁰ B. S. Page,¹⁵ S. K. Pal,⁴⁷ Y. Pandit,¹⁸ Y. Panebratsev,¹¹ S. Y. Panitkin,³ T. Pawlak,⁴⁸ T. Peitzmann,²⁷ V. Perevoztchikov,³ C. Perkins,⁴ W. Peryt,⁴⁸ S. C. Phatak,¹³ M. Planinic,⁵³ J. Pluta,⁴⁸ N. Poljak,⁵³ A. M. Poskanzer,²¹ B. V. K. S. Potukuchi,¹⁷ D. Prindle,⁴⁹ C. Pruneau,⁵⁰ N. K. Pruthi,³⁰ J. Putschke,⁵² R. Raniwala,³⁵ S. Raniwala,³⁵ R. L. Ray,⁴³ R. Redwine,²² R. Reed,⁵ A. Ridiger,²⁵ H. G. Ritter,²¹ J. B. Roberts,³⁶ O. V. Rogachevskiy,¹¹ J. L. Romero,⁵ A. Rose,²¹ C. Roy,⁴¹ L. Ruan,³ M. J. Russcher,²⁷ R. Sahoo,⁴¹ I. Sakrejda,²¹ T. Sakuma,²² S. Salur,²¹ J. Sandweiss,⁵² M. Sarsour,⁴² J. Schambach,⁴³ R. P. Scharenberg,³³ N. Schmitz,²³ J. Seger,⁹ I. Selyuzhenkov,¹⁵ P. Seyboth,²³ A. Shabetai,¹⁶ E. Shahaliev,¹¹ M. Shao,³⁸ M. Sharma,⁵⁰ S. S. Shi,⁵¹ X-H. Shi,⁴⁰ E. P. Sichtermann,²¹ F. Simon,²³ R. N. Singaraju,⁴⁷ M. J. Skoby,³³ N. Smirnov,⁵² R. Snellings,²⁷ P. Sorensen,³ J. Sowinski,¹⁵ H. M. Spinka,¹ B. Srivastava,³³ A. Stadnik,¹¹ T. D. S. Stanislaus,⁴⁶ D. Staszak,⁶ M. Strikhanov,²⁵ B. Stringfellow,³³ A. A. P. Suaide,³⁷ M. C. Suarez,⁸ N. L. Subba,¹⁸ M. Sumner,¹⁰ X. M. Sun,²¹ Y. Sun,³⁸ Z. Sun,²⁰ B. Surrow,²² T. J. M. Symons,²¹ A. Szanto de Toledo,³⁷ J. Takahashi,⁷ A. H. Tang,³ Z. Tang,³⁸ T. Tarnowsky,³³ D. Thein,⁴³ J. H. Thomas,²¹ J. Tian,⁴⁰ A. R. Timmins,² S. Timoshenko,²⁵ D. Tlusty,¹⁰ M. Tokarev,¹¹ T. A. Trainor,⁴⁹ V. N. Tram,²¹ A. L. Trattner,⁴ S. Trentalange,⁶ R. E. Tribble,⁴² O. D. Tsai,⁶ J. Ulery,³³ T. Ullrich,³ D. G. Underwood,¹ G. Van Buren,³ M. van Leeuwen,²⁷ A. M. Vander Molen,²⁴ J. A. Vanfossen, Jr.,¹⁸ R. Varma,¹⁴ G. M. S. Vasconcelos,⁷ I. M. Vasilevski,¹² A. N. Vasiliev,³² F. Videbaek,³ S. E. Vigdor,¹⁵ Y. P. Viyogi,¹³ S. Vokal,¹¹ S. A. Voloshin,⁵⁰ M. Wada,⁴³ W. T. Waggoner,⁹ M. Walker,²² F. Wang,³³ G. Wang,⁶ J. S. Wang,²⁰ Q. Wang,³³ X. Wang,⁴⁴ X. L. Wang,³⁸ Y. Wang,⁴⁴ G. Webb,¹⁹ J. C. Webb,⁴⁶ G. D. Westfall,²⁴ C. Whitten Jr.,⁶ H. Wieman,²¹ S. W. Wissink,¹⁵ R. Witt,⁴⁵ Y. Wu,⁵¹ W. Xie,³³ N. Xu,²¹ Q. H. Xu,³⁹ Y. Xu,³⁸ Z. Xu,³ Yang,²⁰ P. Yepes,³⁶ I-K. Yoo,³⁴ Q. Yue,⁴⁴ M. Zawisza,⁴⁸ H. Zbroszczyk,⁴⁸ W. Zhan,²⁰ S. Zhang,⁴⁰ W. M. Zhang,¹⁸ X. P. Zhang,²¹ Y. Zhang,²¹ Z. P. Zhang,³⁸ Y. Zhao,³⁸ C. Zhong,⁴⁰ J. Zhou,³⁶ R. Zoulkarneev,¹² Y. Zoulkarneeva,¹² and J. X. Zuo⁴⁰

(STAR Collaboration)

- ¹Argonne National Laboratory, Argonne, Illinois 60439, USA
²University of Birmingham, Birmingham, United Kingdom
³Brookhaven National Laboratory, Upton, New York 11973, USA
⁴University of California, Berkeley, California 94720, USA
⁵University of California, Davis, California 95616, USA
⁶University of California, Los Angeles, California 90095, USA
⁷Universidade Estadual de Campinas, Sao Paulo, Brazil
⁸University of Illinois at Chicago, Chicago, Illinois 60607, USA
⁹Creighton University, Omaha, Nebraska 68178, USA
¹⁰Nuclear Physics Institute AS CR, 250 68 Řež/Prague, Czech Republic
¹¹Laboratory for High Energy (JINR), Dubna, Russia
¹²Particle Physics Laboratory (JINR), Dubna, Russia
¹³Institute of Physics, Bhubaneswar 751005, India
¹⁴Indian Institute of Technology, Mumbai, India
¹⁵Indiana University, Bloomington, Indiana 47408, USA
¹⁶Institut de Recherches Subatomiques, Strasbourg, France
¹⁷University of Jammu, Jammu 180001, India
¹⁸Kent State University, Kent, Ohio 44242, USA
¹⁹University of Kentucky, Lexington, Kentucky, 40506-0055, USA
²⁰Institute of Modern Physics, Lanzhou, China
²¹Lawrence Berkeley National Laboratory, Berkeley, California 94720, USA
²²Massachusetts Institute of Technology, Cambridge, MA 02139-4307, USA
²³Max-Planck-Institut für Physik, Munich, Germany
²⁴Michigan State University, East Lansing, Michigan 48824, USA
²⁵Moscow Engineering Physics Institute, Moscow Russia
²⁶City College of New York, New York City, New York 10031, USA
²⁷NIKHEF and Utrecht University, Amsterdam, The Netherlands
²⁸Ohio State University, Columbus, Ohio 43210, USA
²⁹Old Dominion University, Norfolk, VA, 23529, USA
³⁰Panjab University, Chandigarh 160014, India
³¹Pennsylvania State University, University Park, Pennsylvania 16802, USA
³²Institute of High Energy Physics, Protvino, Russia
³³Purdue University, West Lafayette, Indiana 47907, USA
³⁴Pusan National University, Pusan, Republic of Korea
³⁵University of Rajasthan, Jaipur 302004, India
³⁶Rice University, Houston, Texas 77251, USA
³⁷Universidade de Sao Paulo, Sao Paulo, Brazil
³⁸University of Science & Technology of China, Hefei 230026, China
³⁹Shandong University, Jinan, Shandong 250100, China
⁴⁰Shanghai Institute of Applied Physics, Shanghai 201800, China
⁴¹SUBATECH, Nantes, France
⁴²Texas A&M University, College Station, Texas 77843, USA
⁴³University of Texas, Austin, Texas 78712, USA
⁴⁴Tsinghua University, Beijing 100084, China
⁴⁵United States Naval Academy, Annapolis, MD 21402, USA
⁴⁶Valparaiso University, Valparaiso, Indiana 46383, USA
⁴⁷Variable Energy Cyclotron Centre, Kolkata 700064, India
⁴⁸Warsaw University of Technology, Warsaw, Poland
⁴⁹University of Washington, Seattle, Washington 98195, USA
⁵⁰Wayne State University, Detroit, Michigan 48201, USA
⁵¹Institute of Particle Physics, CCNU (HZNU), Wuhan 430079, China
⁵²Yale University, New Haven, Connecticut 06520, USA
⁵³University of Zagreb, Zagreb, HR-10002, Croatia

(Dated: March 25, 2019)

We present a systematic analysis of two-pion interferometry in Au+Au collisions at $\sqrt{s_{NN}} = 62.4$ GeV and Cu+Cu collisions at $\sqrt{s_{NN}} = 62.4$ and 200 GeV using the STAR detector at RHIC. The multiplicity and transverse momentum dependences of the extracted femtoscopic radii are studied. The scaling of the apparent freeze-out volume with charged particle multiplicity is studied for the RHIC energy domain. The multiplicity scaling of the measured radii is found to be independent of colliding system and collision energy.

I. INTRODUCTION

One of the definitive predictions of quantum chromodynamics (QCD) is that at sufficiently high temperature

or density [1], strongly interacting matter will be in a

state with colored degrees of freedom, quarks and gluons. The central goal of the experiments with relativistic heavy-ion collisions is to create and study this form of matter, called the quark-gluon plasma (QGP), which might have existed in the microsecond old universe. Numerous experimental observables have been proposed as signatures of QGP creation in heavy-ion collisions [2]. One of the predictions is based on the expectation that the increased number of degrees of freedom associated with the color deconfined state, increases the entropy of the system which should survive subsequent hadronization and freeze-out. The increased entropy is expected to lead to an increased spatial extent and duration of particle emission, thus providing a significant probe for the QGP phase transition [3, 4].

The information about the space-time structure of the emitting source can be extracted with intensity interferometry techniques [5]. This method, popularly known as Hanbury-Brown Twiss (HBT) correlations, was originally developed to measure angular sizes of distant stars [6]. The momentum correlations of the produced particles from hadronic sources however include dynamical as well as interference effects, hence the term *femtoscopy* [7] is more appropriate. The primary goal of femtoscopy, performed at mid-rapidity and low transverse momentum, is to study the space-time size of the emitting source and freeze-out processes of the dynamically evolving collision fireball. Femtosopic correlations have been successfully studied in most of the heavy-ion experiments (see [8] for a recent review).

Experimentally, the two-particle correlation function is obtained from the ratio,

$$C(\vec{q}, \vec{K}) = \frac{A(\vec{q}, \vec{K})}{B(\vec{q}, \vec{K})}, \quad (1)$$

where $A(\vec{q}, \vec{K})$ is the pair distribution for particles with relative momentum $\vec{q} = \vec{p}_1 - \vec{p}_2$ and average momentum $\vec{K} = (\vec{p}_1 + \vec{p}_2)/2$ from the same event, and $B(\vec{q}, \vec{K})$ is the corresponding distribution for pairs of particles taken from different events [9, 10]. The correlation function is normalized to unity at large \vec{q} . With the availability of high statistics data and development of new techniques, it has become possible to have a three-dimensional decomposition of \vec{q} [11, 12, 13], providing better insight into the collision geometry.

Previous femtosopic measurements at RHIC in Au+Au collisions at $\sqrt{s_{NN}} = 130$ GeV [14, 15] and 200 GeV [16, 17] obtained qualitatively similar source sizes. However, detailed comparisons with smaller colliding systems and energies are required in order to understand the dynamics of the source during freeze-out. The crucial information provided from such Bose-Einstein correlation studies with pions will help to improve our understanding of the reaction mechanisms and to constrain theoretical models of heavy ion collisions [18, 19, 20, 21, 22, 23, 24, 25].

In this paper we present a systematic analysis of two-pion interferometry in Au+Au collisions at $\sqrt{s_{NN}} =$

62.4 GeV and Cu+Cu collisions at $\sqrt{s_{NN}} = 62.4$ GeV and 200 GeV using the Solenoidal Tracker at RHIC (STAR) detector at the Relativistic Heavy Ion Collider (RHIC). The article is organized as follows : Section II explains the detector set-up, along with the necessary event, particle and pair cuts. In Section III, the analysis and construction of the correlation function is discussed. The presented results are compared with previous STAR measurements for Au+Au collisions at $\sqrt{s_{NN}} = 200$ GeV in Section IV. This section also includes a compilation of freeze-out volume estimates for all available heavy ion results from AGS, SPS and RHIC. Section V contains a summary and conclusions.

II. EXPERIMENTAL SETUP, EVENT AND PARTICLE SELECTION

A. The STAR detector and Trigger details

The STAR detector [26], which has large acceptance and is azimuthally symmetric, consists of several detector sub-systems used in conjunction with a solenoidal magnet. In the present study, the central Time Projection Chamber (TPC) provided the main information used for track reconstruction. It is 4.2 m long and 4 m in diameter. The TPC covers the pseudo-rapidity region $|\eta| < 1.8$ with full azimuthal coverage ($-\pi < \phi < \pi$). It is a gas chamber filled with P10 gas (10% methane, 90% argon), with inner and outer radii of 50 and 200 cm, respectively, in a uniform electric field ≈ 135 V/cm. The paths of the particles passing through the gas are reconstructed from the release of secondary electrons that drift to the readout end caps at both ends of the chamber. The readout system is based on multi-wire proportional chambers, with readout pads. There are 45 pad-rows between the inner and the outer radii of the TPC.

A minimum bias trigger is obtained using the charged particle hits from an array of scintillator slats arranged in a barrel, called the Central Trigger Barrel, surrounding the TPC, two zero-degree hadronic calorimeters at ± 18 m from the detector center along the beam line, and two Beam-Beam Counters. The Zero-Degree Calorimeters (ZDCs) [27] measure neutrons at beam rapidity which originate from the break-up of the colliding nuclei. The centrality determination in this analysis uses the uncorrected multiplicity of charged particles in the pseudo-rapidity region $|\eta| < 0.5$ (N_{ch}^{TPC}), as measured by the TPC. In this analysis for Au+Au and Cu+Cu collisions the minimum bias trigger settings and taken at full magnetic field, were used.

B. Event and Centrality Selection

For this analysis we selected events with a collision vertex within ± 30 cm measured along the beam axis from

TABLE I: Centrality selection in terms of percentage cross-section, number of participating nucleons and number of binary collisions for Au+Au at $\sqrt{s_{NN}} = 62.4$ GeV

% cross-section	N_{ch}^{TPC}	$\langle N_{part} \rangle$	$\langle N_{coll} \rangle$
0-5	>373	$347.3^{+4.3}_{-3.7}$	$904^{+67.7}_{-62.4}$
5-10	372-313	$293.3^{+7.3}_{-5.6}$	$713.7^{+63.7}_{-54.8}$
10-20	312-222	$229.0^{+9.2}_{-7.7}$	$511.8^{+54.9}_{-48.2}$
20-30	221-154	$162.0^{+10.0}_{-9.5}$	$320.9^{+43.0}_{-39.2}$
30-40	153-102	$112.0^{+9.6}_{-9.1}$	$193.5^{+30.4}_{-31.4}$
40-50	101-65	$74.2^{+9.0}_{-8.5}$	$109.3^{+22.1}_{-21.8}$
50-60	64-38	$45.8^{+7.0}_{-7.1}$	$56.6^{+15.0}_{-14.3}$
60-70	37-20	$25.9^{+5.6}_{-5.6}$	$26.8^{+8.8}_{-9.0}$
70-80	19-9	$13.0^{+3.4}_{-4.6}$	$11.2^{+3.7}_{-4.8}$

TABLE II: Centrality selection in terms of percentage cross-section, number of participating nucleons and number of binary collisions for Cu+Cu at $\sqrt{s_{NN}} = 200$ GeV

% cross-section	N_{ch}^{TPC}	$\langle N_{part} \rangle$	$\langle N_{coll} \rangle$
0-10	>139	$99.0^{+1.5}_{-1.2}$	$188.8^{+15.4}_{-13.4}$
10-20	138-98	$74.6^{+1.3}_{-1.0}$	$123.6^{+9.4}_{-8.3}$
20-30	97-67	$53.7^{+0.9}_{-0.7}$	$77.6^{+5.4}_{-4.7}$
30-40	66-46	$37.8^{+0.7}_{-0.5}$	$47.7^{+2.8}_{-2.7}$
40-50	45-30	$26.2^{+0.5}_{-0.4}$	$29.2^{+1.6}_{-1.4}$
50-60	29-19	$17.2^{+0.4}_{-0.2}$	$16.8^{+0.7}_{-0.7}$

the center of the TPC. This event selection was applied to all the data sets discussed here.

The events were further binned according to the collision centrality, where the centrality is characterized according to the measured multiplicity of charged hadrons within the pseudo-rapidity range $|\eta| < 0.5$. In Table I, we give the centrality bins for Au+Au at $\sqrt{s_{NN}} = 62.4$ GeV along with the multiplicity bin, average number of participating nucleons and average number of binary collisions [28, 29]. For the present analysis we chose six centrality bins corresponding to 0-5%, 5-10%, 10-20%, 20-30%, 30-50%, 50-80% of the total hadronic cross-section. A dataset of 2 million minimum-bias events which passed the event cuts was used in the analysis.

TABLE III: Centrality selection in terms of percentage cross-section, number of participating nucleons and number of binary collisions for Cu+Cu at $\sqrt{s_{NN}} = 62.4$ GeV

% cross-section	N_{ch}^{TPC}	$\langle N_{part} \rangle$	$\langle N_{coll} \rangle$
0-10	>101	$96.4^{+1.1}_{-2.6}$	$161.8^{+12.1}_{-13.5}$
10-20	100-71	$72.1^{+0.6}_{-1.9}$	$107.5^{+6.3}_{-8.6}$
20-30	70-49	$51.8^{+0.5}_{-1.2}$	$68.4^{+3.6}_{-4.7}$
30-40	48-33	$36.2^{+0.4}_{-0.8}$	$42.3^{+1.9}_{-2.6}$
40-50	32-22	$24.9^{+0.4}_{-0.6}$	$25.9^{+1.0}_{-1.5}$
50-60	21-14	$16.3^{+0.4}_{-0.3}$	$15.1^{+0.6}_{-0.6}$

Tables II and III list the six centrality bins for Cu+Cu at $\sqrt{s_{NN}} = 200$ GeV and 62.4 GeV corresponding to 0-10%, 10-20%, 20-30%, 30-40%, 40-50%, 50-60% of the total hadronic cross-section. The number events used was 15 million and 24 million for 62.4 GeV and 200 GeV Cu+Cu datasets, respectively after the event cuts.

C. Particle Selection

We selected tracks in the rapidity region $|y| < 0.5$. The particle identification was performed by correlating the specific ionization of particles in the TPC gas with their measured momenta. For this analysis pions were selected by requiring the specific ionization to be within 2 standard deviations from their theoretical Bethe-Bloch value. For the removal of kaons and protons which could satisfy this condition, particles were also required to be further than 2 standard deviations from the Bethe-Bloch value for kaons and protons. The cuts which we used were similar to those in our previous analysis of Au+Au collisions at $\sqrt{s_{NN}} = 200$ GeV [17] since the detector setup was identical.

D. Pair Cuts

The splitting and merging of tracks needs to be understood and studied at pair level. The track splitting causes an enhancement of pairs in the low relative momentum q and to address this problem we have also another set of quality cut on the tuning of this Splitting Level(SL). The value of $SL = -0.5$ clearly shows two separate tracks and it has been studied that $SL \leq 0.6$ is stable. Henceforth from the study of the correlation function with q_{inv} we have set the SL from -0.5 to 0.6 throughout this present analysis. By requiring that the fraction of merged hits to be less than 10 % for every pair entering the correla-

tion function, the track merging was found to be removed completely.

In the present analysis, we used the same cuts to remove splitting and merging as was used for Au+Au collisions at $\sqrt{s_{\text{NN}}} = 200$ GeV [17]. Charged particle tracks reconstructed on the TPC used for this analysis were accepted, if they satisfied the requirements to have hits on at least 15 pad rows, as the shorter tracks maybe from other broken track fragments. The track pairs were required to have an average transverse momentum ($k_{\text{T}} = (|\vec{p}_{1\text{T}} + \vec{p}_{2\text{T}}|)/2$) in one of 4 bins corresponding to [150,250] MeV/c, [250,350] MeV/c, [350,450] MeV/c and [450,600] MeV/c. The results are presented and discussed as a function of k_{T} as well as $m_{\text{T}} (= \sqrt{k_{\text{T}}^2 + m_{\pi}^2})$ in each of those bins.

III. ANALYSIS METHOD

A. Correlation function

The two particle correlation function is constructed based on Eq.(1) where the measured distribution in the numerator corresponds to pairs from the same event whereas the denominator was obtained from mixed events. The latter background pairs were constructed from mixed events [9] where each particle in a given event was mixed with all particles from other events within a collection of ten similar events. The similar events were selected within each centrality bin and further binned to have relative primary vertex z positions within 10 cm.

B. Bertsch-Pratt Parametrizations and Coulomb interactions

We decompose the relative momentum \vec{q} according to the Bertsch-Pratt (or “out-side-long”) convention [11, 12, 13, 30, 31]. The relative momentum \vec{q} is decomposed into the variables q_{long} along the beam direction, q_{out} parallel to the transverse momentum of the pair $\vec{k}_{\text{T}} = (\vec{p}_{1\text{T}} + \vec{p}_{2\text{T}})/2$, and q_{side} perpendicular to q_{long} and q_{out} .

In addition to the correlation arising from quantum statistics of two identical (boson) particles, correlations can also arise from two-particle final state interactions even if the symmetry-based correlations are absent [32, 33, 34]. For identical pions the effects of strong interactions are negligible but the long range Coulomb repulsion causes a suppression of the measured correlation function at small \vec{q} .

In this paper we followed the procedure used in our previous analysis of Au+Au collisions at $\sqrt{s_{\text{NN}}} = 200$ GeV [17]. For an azimuth integrated analysis at mid-rapidity in the longitudinal co-moving system (LCMS) the correlation function in Eq. (1) can be decomposed as [8, 35]:

$$C(q_{\text{out}}, q_{\text{side}}, q_{\text{long}}) = (1-\lambda) +$$

$$\lambda K_{\text{Coul}}(q_{\text{inv}})(1 + e^{-q_{\text{out}}^2 R_{\text{out}}^2 - q_{\text{side}}^2 R_{\text{side}}^2 - q_{\text{long}}^2 R_{\text{long}}^2}), \quad (2)$$

where K_{Coul} is to a good approximation the squared non-symmetrized Coulomb wave function integrated over a Gaussian source (corresponding to the LCMS Gaussian radii $R_{\text{out}}, R_{\text{side}}, R_{\text{long}}$). It is averaged over the angles of the relative momentum \vec{q}^* in the pair rest frame, and thus depending on $|\vec{q}^*| = q_{\text{inv}}$ only. Considering experimental identification is perfect and the source is purely chaotic, λ represents the fraction of correlated pairs [36].

We assumed a spherical Gaussian source of 5 fm for Au+Au collisions at $\sqrt{s_{\text{NN}}} = 62.4$ GeV, whereas a 3 fm correction was used for Cu+Cu collisions at $\sqrt{s_{\text{NN}}} = 62.4$ and 200 GeV in the present analysis. The first term $(1 - \lambda)$ in Eq.(2) accounts for those pairs which do not interact or interfere and the second term represents those pairs where both Bose-Einstein effects and Coulomb interactions are present [17].

C. Systematic Uncertainties

Similar to previously published by STAR pion interferometry analysis for Au+Au collisions at $\sqrt{s_{\text{NN}}} = 200$ GeV [17] we studied several sources of systematic errors. The following effects were considered - track merging, track splitting, size of the source used for Coulomb correction, particle identification purity and pair acceptance effects for pions of different charges. The estimated systematic errors are less than 10% for all radii, in all centralities and k_{T} bins for the presented datasets and are similar to those in [17]. This was expected since the detector setup was identical and similar particle and pair selection cuts were used for Au+Au and Cu+Cu collisions. Please note that the Figures presented in this paper for Au+Au collisions at $\sqrt{s_{\text{NN}}} = 62.4$ GeV and Cu+Cu collisions at $\sqrt{s_{\text{NN}}} = 62.4$ and 200 GeV are only with statistical errors.

IV. RESULTS AND DISCUSSION

A. Au+Au collisions at $\sqrt{s_{\text{NN}}} = 62.4$ GeV

The correlation function described in Eq.(2) was fitted to the 3D correlation data for Au+Au collisions at $\sqrt{s_{\text{NN}}} = 62.4$ GeV for each centrality and m_{T} bins as defined above. The analysis was performed separately for $\pi^+\pi^+$ and $\pi^-\pi^-$ pairs. The final histograms for the like-sign pairs were summed up in order to increase the statistics as they do not show appreciable differences. Figure 1 gives the results for $R_{\text{out}}, R_{\text{side}}, R_{\text{long}}, \lambda$ and the ratio, $R_{\text{out}}/R_{\text{side}}$. The three femtoscopic radii increase with increasing centrality as expected, whereas the values of the λ parameter and the $R_{\text{out}}/R_{\text{side}}$ ratio exhibit no clear centrality dependences.

We observe that for all centralities the three femtoscopic radii decrease with increasing m_{T} whereas the λ

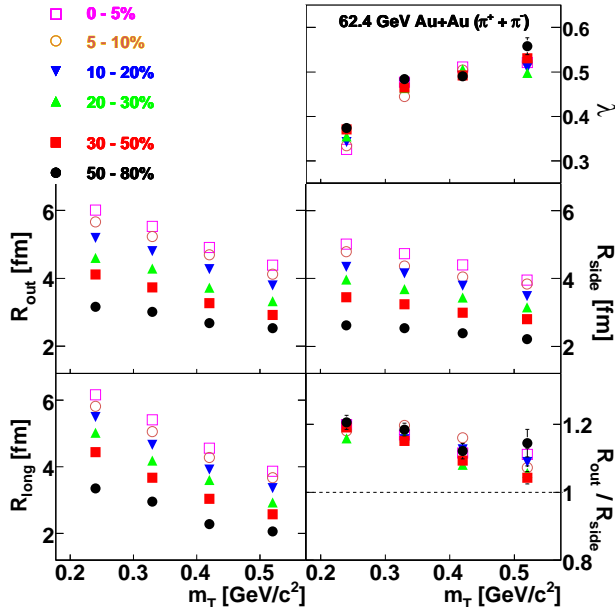


FIG. 1: (Color Online) The femtoscopic parameters vs m_T for 6 different centralities for Au+Au collisions at $\sqrt{s_{NN}} = 62.4$ GeV. Only statistical errors are shown.

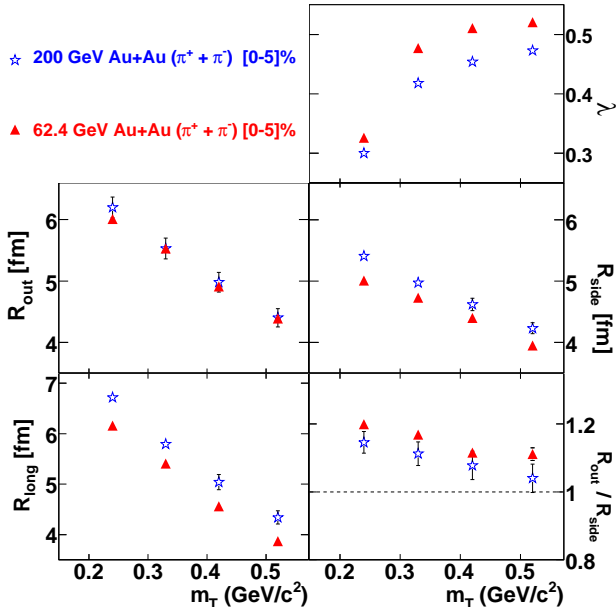


FIG. 2: (Color Online) The comparison of femtoscopic measurements of Au+Au collisions at $\sqrt{s_{NN}} = 200$ GeV and 62.4 GeV for 0-5% most central events. The 200 GeV results are from [17].

parameter increases with m_T . Such behavior is consistent with our previous measurements at $\sqrt{s_{NN}} = 200$ GeV [17]. The increase of parameter λ with m_T is due to the decreasing contribution of pions produced from long-lived resonance decays at higher transverse momenta. For comparison, in Fig. 2 we show the results for Au+Au

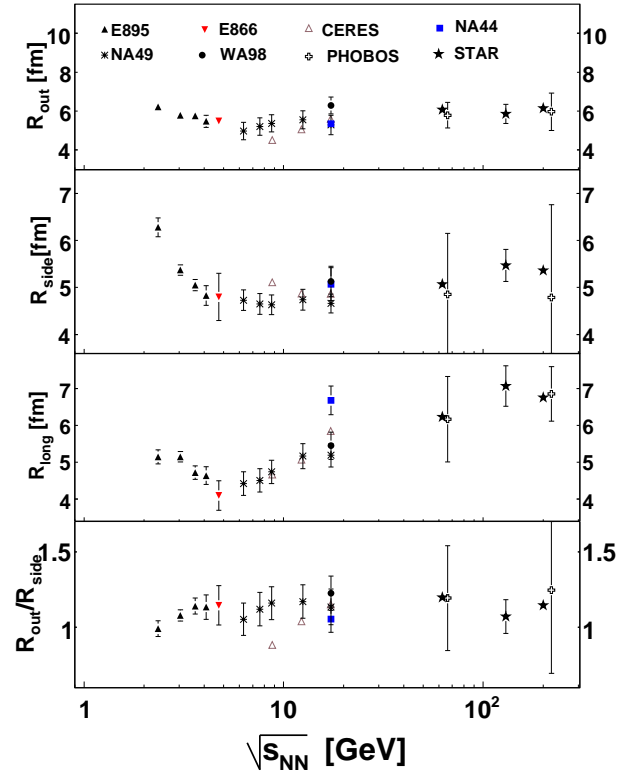


FIG. 3: (Color Online) The energy dependence of femtoscopic parameters for AGS, SPS and RHIC from Refs [14, 17, 47, 48, 49, 50, 51, 52, 53, 54]. Energy dependences of pion femtoscopic parameters for central Au+Au, Pb+Pb and Pb+Au collisions are shown for mid-rapidity and $\langle k_T \rangle \sim 0.2-0.3$ GeV/c. Error bars on NA44, NA49, CERES, PHOBOS and STAR results at $\sqrt{s_{NN}} = 130$ and 200 GeV include systematic uncertainties; error bars on other results are statistical only. The PHOBOS results from [47] for $\sqrt{s_{NN}} = 62.4$ and 200 GeV are slightly shifted horizontally to improve presentation.

collisions at $\sqrt{s_{NN}} = 62.4$ GeV and 200 GeV for the most central collisions. We observe that the R_{out} values are similar for both cases but there is a difference in the values of R_{side} and R_{long} . The R_{out}/R_{side} ratio decreases with increasing m_T but the values are higher for $\sqrt{s_{NN}} = 62.4$ GeV compared to the results for $\sqrt{s_{NN}} = 200$ GeV.

The behavior observed for the three femtoscopic radii is qualitatively consistent with models with collective flow [37, 38, 39]. This collective expansion results in position-momentum correlations in both transverse and longitudinal directions. In an expanding source, the correlation between the space-time points where the pions are emitted and their energy-momentum produce a characteristic dependence of femtoscopic radii on m_T [8, 12, 22, 40, 41, 42, 43, 44, 45]. The decrease in the “out” and “side” components can be described by transverse flow [17, 22, 40, 42], and the decrease in the “long” component by longitudinal flow [17, 41, 42, 46].

B. Energy dependence of femtoscopic radii

In Fig. 3 we present the energy dependences of the three femtoscopic radii and the ratio $R_{\text{out}}/R_{\text{side}}$ for the available data from AGS, SPS and RHIC. The results are compiled for Au+Au, Pb+Pb and Pb+Au collisions at mid-rapidity and for $\langle k_T \rangle \sim 0.2\text{-}0.3$ GeV/c. We include the present measurements for Au+Au collisions at $\sqrt{s_{\text{NN}}} = 62.4$ GeV. The quality of the data and the error bars show significant improvement for the present STAR results compared to those reported by the PHOBOS experiment [47] at the same energy. PHENIX results were not plotted because they were reported for broader centrality bins. WA97 results were also omitted because they were measured at higher transverse momenta.

Comparative studies are a necessary part of searches for nontrivial structures in the excitation function which might arise from a possible phase transition [3]. The radius parameter R_{side} has the most direct correlation with the source geometry whereas R_{out} encodes both geometry and time scale. Experimental results show that R_{side} decreases at AGS energies and then displays a modest rise with collision energy from SPS to RHIC. R_{long} increases with collision energy after an initial decrease at lowest AGS energies. For R_{out} the change is very small.

Hydrodynamic calculations [3, 4] predict an enhancement in the ratio of $R_{\text{out}}/R_{\text{side}}$ with increasing beam energy. The experimental results show no such behavior. The measured ratios are better reproduced by the AMPT (A Multi-Phase Transport) model [55], however the individual predicted radii have a steeper decrease compared to the experimental data [8]. An alternate model using a relativistic quantum mechanical treatment of opacity and the refractive index is capable of reproducing the observed results [56] but strongly depends on the assumed initial conditions and neglects the time dependence of the corresponding optical potential. Initial hydrodynamic calculations [57] including viscosity offer another possible explanation for the above deviation between the data and model calculations as recently shown [58]. According to recent hydrodynamic calculations, the femtoscopic radii can be described either by using the initial Gaussian density profile [59] or by including the combination of several effects: pre-thermal acceleration, a stiffer equation of state, and adding viscous corrections [60]. Other recent studies with a granular source model [61] also obtain a better description of the experimental measurements of pion femtoscopic radii.

C. Cu+Cu collisions at $\sqrt{s_{\text{NN}}} = 62.4$ and 200 GeV

The correlation functions were constructed for Cu+Cu collisions at $\sqrt{s_{\text{NN}}} = 62.4$ GeV and 200 GeV. The extracted femtoscopic radii, R_{out} , R_{side} , R_{long} along with the λ parameter and the ratio $R_{\text{out}}/R_{\text{side}}$ are presented in Figs. 4 and 5 for the 62.4 and 200 GeV data, respectively. The results are presented for six different central-

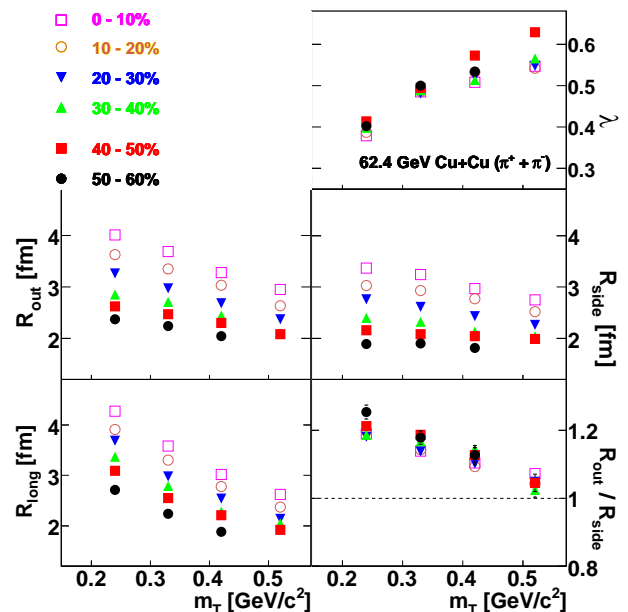


FIG. 4: (Color Online) Femtoscopic parameters vs m_T for six centralities for Cu+Cu collisions at $\sqrt{s_{\text{NN}}} = 62.4$ GeV.

ities and four m_T bins. The highest k_T bin [450 - 600] MeV/c of the most peripheral centrality (50 - 60 %) in Cu+Cu collisions at $\sqrt{s_{\text{NN}}} = 62.4$ GeV is omitted due to inadequate statistics for decomposition with the Bertsch-Pratt parametrization. For both collision energies the three femtoscopic radii increase with increasing centrality whereas the λ parameter shows no centrality dependence. The m_T dependences of the femtoscopic radii are similar to that for Au+Au collisions. The $R_{\text{out}}/R_{\text{side}}$ ratios exhibit no clear centrality dependence for both energies.

D. Comparison of femtoscopic radii for Cu+Cu and Au+Au collisions

In Fig. 6 the femtoscopic source parameters λ , R_{out} , R_{side} , R_{long} and the ratio $R_{\text{out}}/R_{\text{side}}$ for central (0-5%) Au+Au collisions at $\sqrt{s_{\text{NN}}} = 200$ GeV [17] are compared with central (0-10%) Cu+Cu collisions at same beam energy. As expected, the femtoscopic radii for Cu+Cu collisions are smaller than for Au+Au collisions at the same beam energy. It is interesting that the values of the ratio $R_{\text{out}}/R_{\text{side}}$ are similar.

In Fig. 7 we extend the comparison of femtoscopic source parameters to include central (0-5%) Au+Au collisions at $\sqrt{s_{\text{NN}}} = 62.4$ GeV, central (0-10%) Cu+Cu collisions at $\sqrt{s_{\text{NN}}} = 62.4$ and 200 GeV, and central (0-15%) $\pi^+\pi^+$ and $\pi^-\pi^-$ correlations from Au+Au collisions at 62.4 GeV from the PHOBOS experiment [47]. The femtoscopic radii for Cu+Cu collisions at $\sqrt{s_{\text{NN}}} = 62.4$ GeV are smaller than those for Au+Au collisions at the same beam energy. The femtoscopic radii for Cu+Cu central collisions are similar for both energies. The variation of

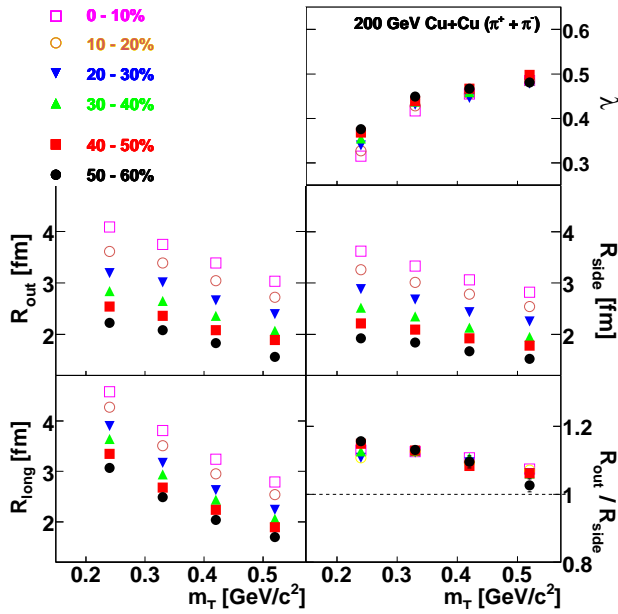


FIG. 5: (Color Online) Femsotopic parameters vs m_T for six centralities for Cu+Cu collisions at $\sqrt{s_{NN}} = 200$ GeV.

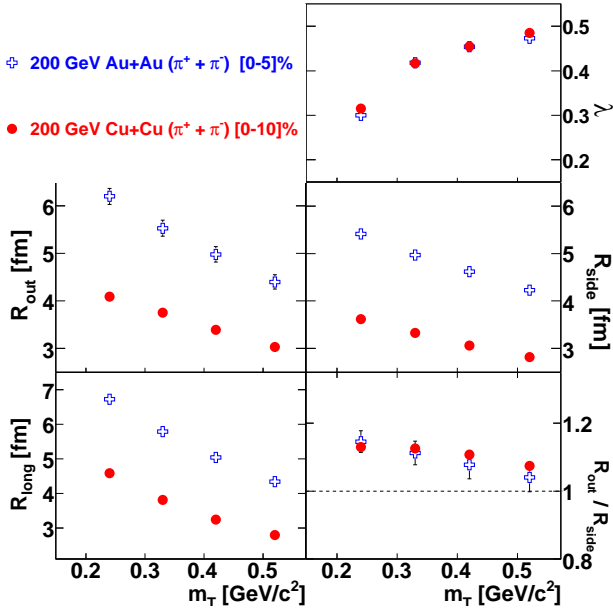


FIG. 6: (Color Online) The comparison of System size dependence in femsotopic measurements of STAR Au+Au and Cu+Cu collisions at $\sqrt{s_{NN}} = 200$ GeV. The Au+Au results are from [17].

ratio R_{out}/R_{side} with m_T is similar for the Au+Au and Cu+Cu collision data.

In Fig. 8 we present the m_T dependences of the ratios of femsotopic radii for the most-central Au+Au and Cu+Cu collisions at $\sqrt{s_{NN}} = 200$ and 62.4 GeV. Ratios for the same colliding ion systems are close to unity whereas ratios of radii for Au+Au to Cu+Cu collisions

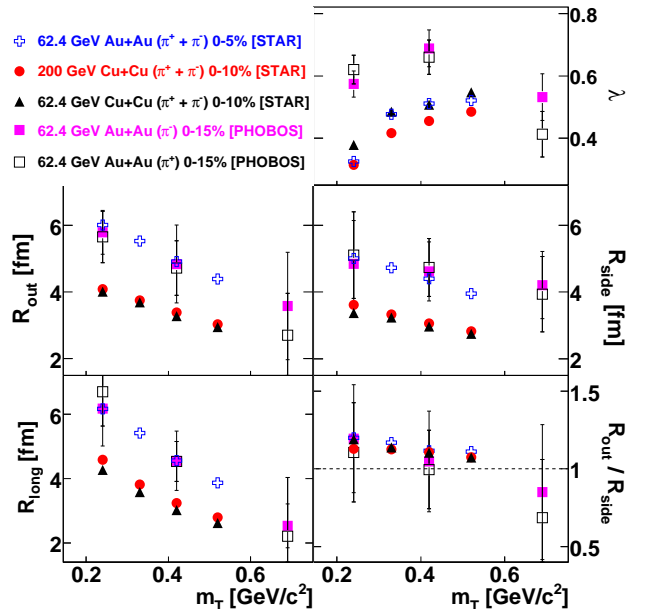


FIG. 7: (Color Online) The comparison of femsotopic measurements of STAR Cu+Cu collisions at $\sqrt{s_{NN}} = 200$ and 62.4 GeV and Au+Au collisions at $\sqrt{s_{NN}} = 62.4$ GeV. The PHOBOS results [47] for positive and negative pions in Au+Au collisions at $\sqrt{s_{NN}} = 62.4$ GeV are compared with STAR results.

are ~ 1.5 . Although the individual radii decrease significantly with increasing m_T the ratios in Fig. 8 show that the femsotopic radii for Au+Au and Cu+Cu collisions at 62.4 and 200 GeV share a common m_T dependence. This result can be understood in terms of models [56, 62] which use participant scaling to predict the femsotopic radii in Cu+Cu collisions, from the measured radii for Au+Au collisions at $\sqrt{s_{NN}} = 200$ GeV, assuming the radii are proportional to $A^{1/3}$, where A is the atomic mass number of the colliding nuclei.

E. Volume estimates and multiplicity scaling

Estimates of the pion freeze-out volume V_f in terms of the femsotopic radii are provided by the following expressions:

$$V_f \propto R_{side}^2 R_{long} \quad (3a)$$

$$V_f \propto R_{out} R_{side} R_{long}. \quad (3b)$$

However, the correlation lengths (femsotopic radii) decrease with increasing m_T corresponding to an m_T dependent region of homogeneity which, in expanding source models, is smaller than the true collision volume at freeze-out. The volume estimates [Eqs. (3a) and (3b)] are obtained from the lowest m_T bin, corresponding to the k_T region from 150 to 250 MeV/c as discussed in Sec. (IID).

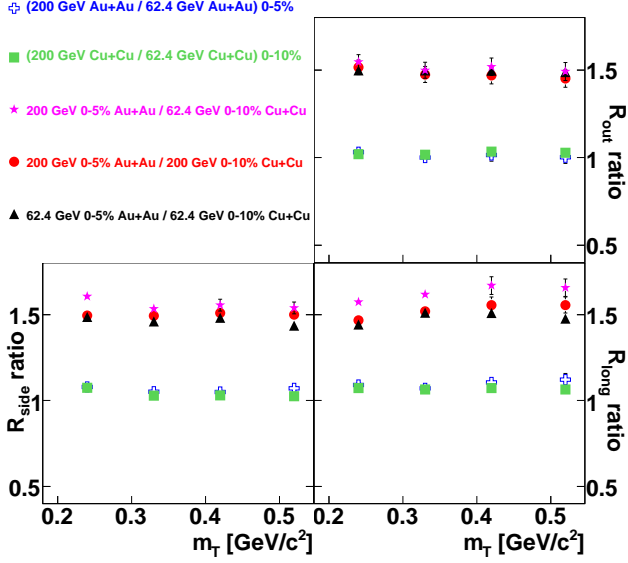


FIG. 8: (Color Online) Ratios of femtosopic radii at top centralities for Au+Au and Cu+Cu collisions at $\sqrt{s_{NN}} = 200$ and 62.4 GeV versus m_T .

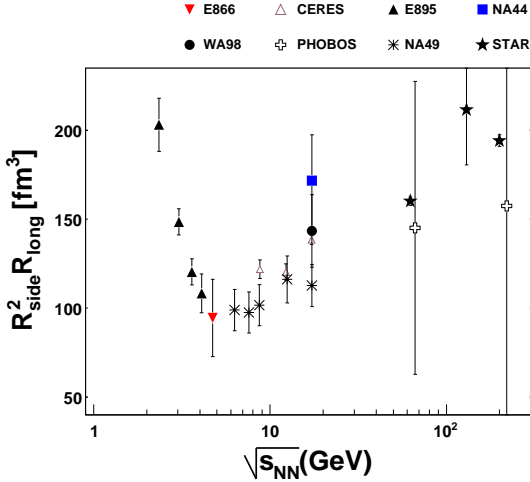


FIG. 9: (Color Online) The energy dependence of the pion freeze-out volume for heavy-ion collision data from the AGS, SPS and RHIC estimated using Eq. (3a). The references are given in Fig. 3.

The V_f measurements using Eq. (3a) as a function of $\sqrt{s_{NN}}$ are presented in Fig. 9 for Au+Au, Pb+Pb and Pb+Au collisions at mid-rapidity and for the lowest k_T bin defined above. The results show two distinct domains: First at the AGS where the observed volumes decreases and the second with a steadily rise within the SPS and RHIC energy regimes.

A detailed description of this non-trivial behavior was suggested in [63] based on the hypothesis of constant mean free path of pions at freeze-out. The explanation

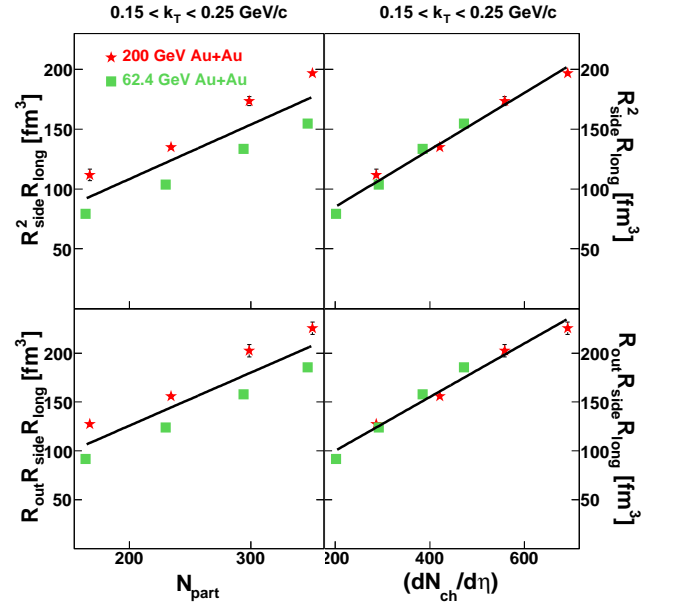


FIG. 10: (Color Online) Pion freeze-out volume estimates as a function of number of participants and charged particle multiplicities for Au+Au at $\sqrt{s_{NN}} = 200$ and 62.4 GeV. The 200 GeV Au+Au collision results are from [17]. The lines in each panel represent linear fits to the data.

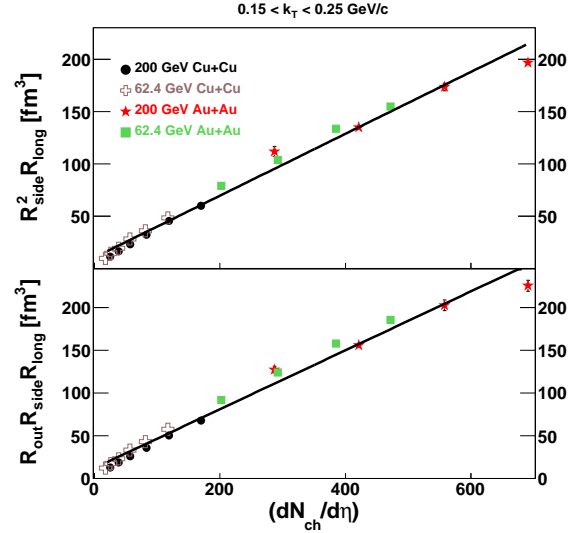


FIG. 11: (Color Online) Pion freeze-out volume estimates as a function of charged particle multiplicity at mid-rapidity for Au+Au and Cu+Cu collisions. The 200 GeV Au+Au collision results are from [17]. The lines in each panel represent linear fits to the data.

provided in [63] defines the pion mean free path, λ_f , as:

$$\lambda_f = \frac{1}{\rho_f \sigma} = \frac{V_f}{N\sigma}, \quad (4)$$

where ρ_f is the freeze-out density and σ is the total cross-section for pions to interact with the surrounding

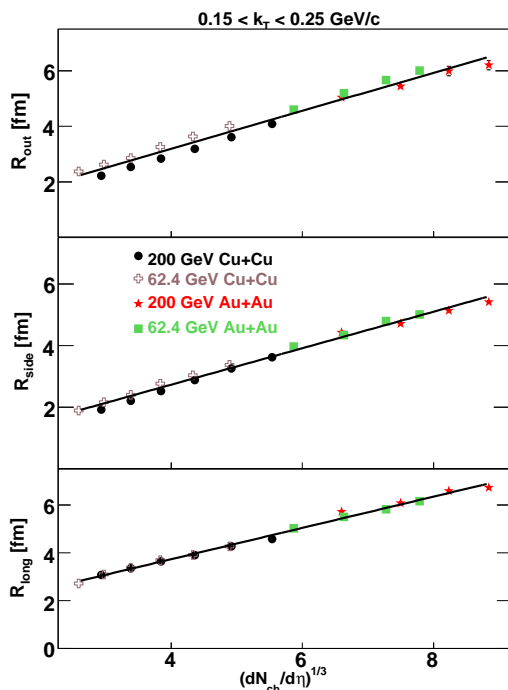


FIG. 12: (Color Online) The pion source radii dependence on charged particle multiplicity for Au+Au and Cu+Cu collisions. The 200 GeV Au+Au collision results are from [17]. The lines represent linear fits to the data.

medium. The freeze-out density can be expressed as the number of particles N in the estimated freeze-out volume V_f , divided by V_f , resulting in the second expression in Eq. (4). The denominator $N\sigma$ can be expanded as the sum of the pion-pion and pion-nucleon contributions. At AGS energies the pion-nucleon term dominates since the pion-proton cross-section is larger than the pion-pion cross-section. Also, the number of nucleons for such energies at mid-rapidity is more than the number of pions. Hence, a decrease in the number of mid-rapidity nucleons leads to a decrease in the observed freeze-out volume (V_f) as a function of \sqrt{s} . At SPS and RHIC energies the pion-pion term dominates the denominator in Eq. (4) due to copious pion production leading to an increase in the observed V_f .

Based on this interpretation we expect the volume estimates in the pion dominated RHIC regime to show a linear dependence on charged particle multiplicity. In Fig. 10 freeze-out volume estimates (using Eqs. (3a) and (3b)) are shown as a function of the number of participants (left panels) and charged particle multiplicity (right panels) for Au+Au collisions at $\sqrt{s_{NN}} = 62.4$ and 200 GeV. The predicted linear increase with charged particle multiplicity is observed. Estimated freeze-out volumes for Au+Au collisions at the same centralities increase with collision energy indicating that N_{part} is not a suitable scaling variable in this case. On the other hand, charged particle multiplicity provides better scaling prop-

erties.

The study of the dependence of the freeze-out volume estimates on charged particle multiplicity continues in Fig. 11 for both the Au+Au and Cu+Cu results at $\sqrt{s_{NN}} = 62.4$ and 200 GeV. Both freeze-out volume estimates for the four collision systems show an approximate, common linear dependence on charged particle multiplicity. The linear dependences of femtoscopic radii with $(dN_{\text{ch}}/d\eta)^{1/3}$ for Au+Au and Cu+Cu collisions at $\sqrt{s_{NN}} = 62.4$ and 200 GeV are shown in Fig. 12. Such dependences [8] are consistent with the assumption of a universal mean-free-path of pions at freeze-out [63].

V. SUMMARY AND CONCLUSIONS

We have presented systematic measurements of pion femtoscopy for Au+Au collisions at $\sqrt{s_{NN}} = 62.4$ GeV and Cu+Cu collisions at $\sqrt{s_{NN}} = 62.4$ and 200 GeV and compared the new results with our previous analysis of Au+Au collisions at $\sqrt{s_{NN}} = 200$ GeV [17]. For all the systems considered, the three extracted femtoscopic radii (R_{out} , R_{side} and R_{long}) increase with centrality, whereas the values of the λ parameter and ratio $R_{\text{out}}/R_{\text{side}}$ are approximately constant with centrality. The three femtoscopic radii decrease with increasing m_T , whereas the λ parameter increases with m_T . The increase of λ with m_T is attributed to the decreasing contribution of pions produced from long-lived resonance decays at higher transverse momentum.

The decrease of femtoscopic radii with increasing m_T can be described by models with collective, transverse and longitudinal expansion or flow. The ratios of femtoscopic radii at top centralities for different colliding systems (Au+Au and Cu+Cu) at $\sqrt{s_{NN}} = 62.4$ and 200 GeV show that the corresponding radii vary with m_T in a similar manner.

The predicted rise of ratio $R_{\text{out}}/R_{\text{side}}$ due to a possible phase transition [3] is not observed for Au+Au and Cu+Cu collisions. The compilation of freeze-out volume estimates V_f as a function of collision energy \sqrt{s} (using Eq. (3a) along with the datasets presented in Fig. 3) shows two distinct domains; V_f decreases at the AGS and steadily rises within the SPS and RHIC energy regimes. At AGS energies the decreasing number of baryons at mid-rapidity leads to a decrease in the observed freeze-out volume (V_f) as a function of \sqrt{s} , after which copious and increasing pion production over the range of beam energies between SPS to RHIC causes the freeze-out volume to rise.

The dependences of the freeze-out volume on number of participants and charged particle multiplicity are observed. Measurements for Au+Au collisions at the same centralities and different energies yield different freeze-out volumes implying that N_{part} is not a suitable scaling variable. The freeze-out volume estimates for all four collision systems presented here show a linear dependence as a function of final charged particle multiplicity which is

consistent with the hypothesis of a universal mean-free-path at freeze-out.

For the systems studied, the multiplicity and k_T dependences of the femtoscopic radii are consistent with previously established trends at RHIC and at lower energies. The radii scale with the collision multiplicity which, in a static model, is consistent with a universal mean-free-path at freeze-out. Such studies establish the baseline systematics against which to compare future femtoscopic studies at the LHC [64].

We thank the RHIC Operations Group and RCF at BNL, and the NERSC Center at LBNL and the resources provided by the Open Science Grid consortium for their

support. This work was supported in part by the Offices of NP and HEP within the U.S. DOE Office of Science, the U.S. NSF, the Sloan Foundation, the DFG cluster of excellence ‘Origin and Structure of the Universe,’ CNRS/IN2P3, RA, RPL, and EMN of France, STFC and EPSRC of the United Kingdom, FAPESP of Brazil, the Russian Ministry of Sci. and Tech., the NNSFC, CAS, MoST, and MoE of China, IRP and GA of the Czech Republic, FOM of the Netherlands, DAE, DST, and CSIR of the Government of India and the Korea Sci. & Eng. Foundation. We wish to thank Polish State Committee for Scientific Research, grant: N202 013 31/0489.

-
- [1] L. D. McLerran and B. Svetitsky, Phys. Lett. B **98**, 195 (1981).
- [2] J. Adams *et al.* [STAR Collaboration], Nucl. Phys. A **757**, 102 (2005).
- [3] D. H. Rischke and M. Gyulassy, Nucl. Phys. A **608**, 479 (1996).
- [4] D. H. Rischke, Nucl. Phys. A **610**, 88C (1996).
- [5] G. Goldhaber, S. Goldhaber, W. Y. Lee and A. Pais, Phys. Rev. **120**, 300 (1960).
- [6] R. Hanbury Brown and R. Q. Twiss, Phil. Mag. **45**, 663 (1954). R. Hanbury Brown and R. Q. Twiss, Nature **178**, 1046 (1956).
- [7] R. Lednicky, arXiv:nucl-th/0212089.
- [8] M. A. Lisa, S. Pratt, R. Soltz and U. Wiedemann, Ann. Rev. Nucl. Part. Sci. **55**, 357 (2005).
- [9] G. I. Kopylov and M. I. Podgoretsky, Sov. J. Nucl. Phys. **15**, 219 (1972) [Yad. Fiz. **15**, 392 (1972)].
- [10] U. W. Heinz and B. V. Jacak, Ann. Rev. Nucl. Part. Sci. **49**, 529 (1999).
- [11] G. Bertsch, M. Gong and M. Tohyama, Phys. Rev. C **37**, 1896 (1988).
- [12] S. Pratt, Phys. Rev. D **33**, 1314 (1986).
- [13] S. Chapman, P. Scotto and U. W. Heinz, Phys. Rev. Lett. **74**, 4400 (1995).
- [14] C. Adler *et al.* [STAR Collaboration], Phys. Rev. Lett. **87**, 082301 (2001).
- [15] K. Adcox *et al.* [PHENIX Collaboration], Phys. Rev. Lett. **88**, 192302 (2002).
- [16] S. S. Adler *et al.* [PHENIX Collaboration], Phys. Rev. Lett. **93**, 152302 (2004).
- [17] J. Adams *et al.* [STAR Collaboration], Phys. Rev. C **71**, 044906 (2005).
- [18] G. Baym, Acta Phys. Polon. B **29**, 1839 (1998).
- [19] S. S. Padula, Braz. J. Phys. **35**, 70 (2005).
- [20] E. V. Shuryak, Phys. Lett. B **44**, 387 (1973).
- [21] L. D. McLerran, FERMILAB-CONF-88-068-T Presented at *Int. Conf. on Physics and Astrophysics of the Quark Gluon Plasma, Bombay, India, Feb 8-12, 1988*
- [22] U. W. Heinz, arXiv:nucl-th/9609029.
- [23] U. A. Wiedemann and U. W. Heinz, Phys. Rept. **319**, 145 (1999).
- [24] U. W. Heinz, Nucl. Phys. A **610**, 264C (1996).
- [25] B. Tomasik and U. A. Wiedemann, arXiv:hep-ph/0210250.
- [26] K. H. Ackermann *et al.* [STAR Collaboration], Nucl. Instrum. Meth. A **499**, 624 (2003).
- [27] C. Adler, A. Denisov, E. Garcia, M. J. Murray, H. Strobele and S. White, Nucl. Instrum. Meth. A **470**, 488 (2001).
- [28] J. Adams *et al.* [STAR Collaboration], Phys. Rev. C **73**, 034906 (2006)
- [29] M. L. Miller, K. Reygers, S. J. Sanders and P. Steinberg, Ann. Rev. Nucl. Part. Sci. **57**, 205 (2007).
- [30] M. I. Podgoretsky, Sov. J. Nucl. Phys. **37**, 272 (1983).
- [31] P. Grassberger, Nucl. Phys. B120, 231 (1977)
- [32] R. Lednicky and V. L. Lyuboshitz, Sov. J. Nucl. Phys. **35**, 770 (1982).
- [33] M. Gyulassy, S. K. Kauffmann and L. W. Wilson, Phys. Rev. C **20**, 2267 (1979).
- [34] D. H. Boal, C. K. Gelbke and B. K. Jennings, Rev. Mod. Phys. **62**, 553 (1990).
- [35] Yu. Sinyukov, R. Lednicky, S. V. Akkelin, J. Pluta and B. Erasmus, Phys. Lett. B **432**, 248 (1998).
- [36] M. A. Lisa and S. Pratt, arXiv:0811.1352 [nucl-ex].
- [37] P. F. Kolb and U. W. Heinz, arXiv:nucl-th/0305084.
- [38] F. Retiere and M. A. Lisa, Phys. Rev. C **70**, 044907 (2004).
- [39] T. Hirano and K. Tsuda, Nucl. Phys. A **715**, 821 (2003).
- [40] B. Tomasik, U. A. Wiedemann and U. W. Heinz, Nucl. Phys. A **663**, 753 (2000).
- [41] U. A. Wiedemann, P. Scotto and U. W. Heinz, Phys. Rev. C **53**, 918 (1996).
- [42] U. A. Wiedemann, Phys. Rev. C **57**, 266 (1998).
- [43] S. Pratt, Phys. Rev. Lett. **53**, 1219 (1984).
- [44] B. R. Schlei and N. Xu, Phys. Rev. C **54**, 2155 (1996).
- [45] B. R. Schlei, U. Ornik, M. Plumer and R. M. Weiner, Phys. Lett. B **293**, 275 (1992).
- [46] A. N. Makhlin and Y. M. Sinyukov, Z. Phys. C **39**, 69 (1988).
- [47] B. B. Back *et al.* [PHOBOS Collaboration], Phys. Rev. C **73**, 031901 (2006).
- [48] L. Ahle *et al.* [E802 Collaboration], Phys. Rev. C **66**, 054906 (2002).
- [49] D. Adamova *et al.* [CERES collaboration], Nucl. Phys. A **714**, 124 (2003).
- [50] M. A. Lisa *et al.* [E895 Collaboration], Phys. Rev. Lett. **84**, 2798 (2000).
- [51] I. G. Bearden *et al.* [NA44 Collaboration], Phys. Rev. C **58**, 1656 (1998).
- [52] C. Alt *et al.* [NA49 Collaboration], Phys. Rev. C **77**,

- 064908 (2008).
- [53] R. A. Soltz *et al.* [E866 Collaboration], Nucl. Phys. A **661**, 439 (1999).
- [54] M. M. Aggarwal *et al.* [WA98 Collaboration], Phys. Rev. C **67**, 014906 (2003).
- [55] Z. W. Lin, C. M. Ko and S. Pal, Phys. Rev. Lett. **89**, 152301 (2002).
- [56] J. G. Cramer, G. A. Miller, J. M. S. Wu and J. H. S. Yoon, Phys. Rev. Lett. **94**, 102302 (2005).
- [57] D. Teaney, Phys. Rev. C **68**, 034913 (2003).
- [58] P. Romatschke, arXiv:nucl-th/0701032.
- [59] W. Florkowski, W. Broniowski, M. Chojnacki and A. Kisiel, arXiv:0811.3761 [nucl-th].
- [60] S. Pratt, arXiv:0811.3363 [nucl-th].
- [61] W. N. Zhang and C. Y. Wong, arXiv:hep-ph/0702120.
- [62] G. A. Miller and J. G. Cramer, J. Phys. G **34**, 703 (2007).
- [63] D. Adamova *et al.* [CERES Collaboration], Phys. Rev. Lett. **90**, 022301 (2003).
- [64] B. Alessandro *et al.* [ALICE Collaboration], J. Phys. G **32**, 1295 (2006).